ADVANCED FUNCTIONAL MATERIALS
www.afm-journal.de

Enhanced Penetration and Retention of CuS-Based Nanosystem Through NIR Light and In Situ Enzyme Response for Improved Tumor Therapy

Fangli Gao, Liang Zhu, Liting Jiang, Jie Zhang, Shenglu Ji, Weihua Gao, Guanglei Ma, Yi Chang, Xiaoming Ma, and Yuming Guo**

The efficient way to increase the therapeutic efficacy of nanomedicines is by encouraging the penetration and enhancing the retention of nanoparticles at the tumor site. However, it is a serious dilemma that small nanoparticles can penetrate deep into the tumor tissue but easily be cleared into the surrounding tissues. In order to solve this dilemma, a smart nanosystem is created to address this problem, ensuring both the effective penetration of tiny nanoparticles (NPs) and their appropriate retention at the tumor site. CuS NPs that is modified with peptides are prepared facilely, and can aggregate in situ through the intermolecular crosslinking reaction catalyzed by the transglutaminase (TGase) abundantly expressed at the tumor site, resulting in an outstanding photothermal effect for tumor therapy. Upon NIR irradiation, the photothermal effect of CuS-K and CuS-Q induced the disintegration of liposomes and prompted the release of CuS-K, CuS-Q, and indocyanine green (ICG). Simultaneously, CuS-K and CuS-Q aggregated under the catalysis of TGase after being internalized by tumor cells to enhance photothermal therapy. The current study provides valuable inspiration to design nanomedicines with prolonged circulation time in the blood system, better penetration, and retention at the tumor site, and multimodal tumor therapy to achieve the desired therapeutic efficacy.

1. Introduction

Despite extensive research on NPs for application in tumor therapy, their therapeutic effectiveness is far from satisfactory. One of the great obstacles is the poor penetration ability of NPs into deep tumor tissues. The extreme complexity of tumor tissues, including tumor cells, tumor blood vessels, extracellular matrix, and metabolic waste, severely impedes the penetration of most NPs.[1] NPs smaller than 10 nm possess the desirable deep penetration ability, unfortunately, they might be easily cleared up.[2–3] The poor accumulation and retention of NPs at the tumor site lead to inadequate therapeutic efficacy.[4] Therefore, it is an essential prerequisite for NPs to penetrate and remain at tumor sites efficiently to exhibit the desired therapeutic efficacy.[5] To address this issue, stimulus-responsive NPs that can aggregate in situ at the tumor site emerged, including various endogenous stimuli (e.g., altered redox, acidic pH, hypoxic, and up-regulated enzymes) and exogenous stimuli (e.g., light and temperature variation).[6–7] Liu and co-workers prepared a nanosystem with the acid-triggered aggregation ability to enhance the gold NPs' accumulation and retention in cancer cells and tumors, which provided a new strategy and insights into fabricating nanoaggregates to magnify the radiosensitive efficiency of nanosystems in cancer radiotherapy.[8] Shi and co-workers developed a type of photo-cross-linkable AuNPs, achieving light-induced aggregation of small AuNPs in vivo and realizing activated photoacoustic imaging and photothermal therapy (PTT) of tumors in live mice.[9] Aggregation-induced retention has undoubtedly been shown to be a successful method for NPs in tumor imaging and therapy.

Some enzymes have been linked to tumor invasion and metastasis in earlier studies.[10] Moreover, enzymes have high specificity and excellent catalytic efficiency for biological processes. Therefore, tremendous interest is drawn to designing nanosystems with specific enzymatic responses to the tumor microenvironment. As an enzyme that exists in the human body and mammals,[11,12] many studies have proved that TGase is highly

F. Gao, L. Jiang, J. Zhang, W. Gao, Y. Chang, Y. Guo
School of Chemistry and Chemical Engineering
Henan Normal University
Xinxiang, Henan 453007, China
E-mail: guoyuming@htu.edu.cn
L. Zhu, G. Ma, X. Ma
Key Laboratory of Green Chemical Media and Reactions
Ministry of Education
Henan Normal University
Xinxiang, Henan 453007, China
E-mail: mxm@htu.edu.cn
S. Ji
The Key Laboratory of Biomedical Material
School of Life Science and Technology
Xinxiang Medical University
Xinxiang 453003, China

The ORCID identification number(s) for the author(s) of this article can be found under https://doi.org/10.1002/adfm.202312182

DOI: 10.1002/adfm.202312182

overexpressed in tumor tissues and is closely related to the metastasis of cancer cells.[13,14] TGase, in contrast to the majority of the highly expressed enzymes in tumors, could catalyze an amine exchange reaction between γ-carboxamide group of glutamine and the ε-amino group of lysine, leading to the inter- or intramolecular crosslinking of the corresponding proteins rather than their digestion.[15–17] Wang and co-workers reported that a series of polypeptides could be induced to aggregate into NPs or gels by TGase inside the TGase-overexpressed tumor cells in situ.[18]

As one of the promising strategies for tumor therapy, PTT has attracted much attention owing to its spatiotemporal addressability, minimal invasiveness, and high therapeutic efficacy.[9,19,20] Generally, the final therapeutic impact of PTT is often largely determined by photothermal agents. Upon being irradiated by light at a certain wavelength, photothermal agents can generate localized heat to cause protein denaturation, DNA damage, and cellular membrane destruction, consequently resulting in selective ablation of tumor tissues.[21–24] CuS NPs have received substantial study due to their biocompatibility, low toxicity, and cheap cost,[25–27] making them ideal nanomedicine options. Additionally, CuS NPs absorb nearinfrared (NIR) light between the wavelengths of 700 and 1100 nm, which can be attributed to the d-d transition of Cu^{2+} ions.[28,29] Consequently, CuS NPs are often considered one of the potential photothermal agents. However, a single PTT is usually insufficient for the complete ablation of cancer cells due to the complex tumor tissues, which induce inadequate heat and uneven heat distribution during the therapy.[30] As a result, it is strongly advised to combine multimodal tumor treatments.[31] Intriguingly, photodynamic therapy (PDT), as another phototherapy, relies on singlet oxygen or free radicals produced by photoconversion to kill tumor cells by apoptosis, which has a better prognosis. And PDT draws a surge of research interest due to its noninvasiveness, spatiotemporal selectivity, and low systemic toxicity.[32]ICG, a powerful light absorber, can elicit PTT and PDT responses and is widely employed to enhance the effects of a combined therapeutic approach.[33,34]

In our previous work, we revealed the good penetration ability of small CuS NPs and explored the anti-tumor effect of the related nanosystem.[35] However, the CuS NPs are still subject to rapid clearance from the tumor site. Herein, small CuS NPs modified with functional peptides pepK (CRKKKR) and pepQ (CRRQQR) were prepared and denoted as CuS-K and CuS-Q, respectively. PepK and pepQ could be catalyzed by TGase to cause an acyl-transfer reaction between the γ-carboxamide group of peptide-bound glutamine and the ε-amino group of peptide-bound lysine, leading to the formation of a stable and proteolysis-resistant ε-(γ-glutamyl) lysine isopeptide bond in intra- or intermolecular protein crosslinks.[36,37] This process catalyzed by TGase could lead to the aggregation of small CuS-K and CuS-Q in situ at the tumor site, which ensured effective retention of small NPs. Furthermore, the CuS-K and CuS-Q were loaded into thermosensitive liposomes containing ICG, forming a smart nanosystem. The liposome facilitated the prolonged circulation of CuS-K and CuS-Q in the bloodstream and delivered them to the tumor site. Upon irradiation by an 808 nm NIR laser, the photothermal effect of CuS NPs could induce the disintegration of liposomes, prompting the release of CuS-K, CuS-Q, and ICG, further penetrating into the deep tumor site, aggregating catalyzed by TGase, and finally killing tumor cells by combining PTT of CuS and PDT of ICG (**Scheme 1**). This nanosystem not only enables the small NPs to efficiently penetrate deep tumor sites but also ensures their considerable accumulation and retention at the tumor site, thus enhancing therapeutic efficacy significantly. Moreover, aggregation was triggered by the intracellular-specific enzyme overexpressed in tumor cells, while the combined PTT and PDT could precisely ablate tumors. This might provide a promising inspiration to construct nanomedicines with ideal penetration, accumulation, and retention abilities at tumor sites to acquire satisfactory tumor therapeutic therapy.

2. Results and Discussion

2.1. Synthesis and Characterization of the CuS-K NPs, CuS-Q NPs, Lipo@ICG@CuS-K NPs, and Lipo@ICG@CuS-Q NPs

First, the K and Q peptides were synthesized using the solid-phase synthetic method and characterized by high-resolution mass spectra (Figures S1 and S2, Supporting Information). Next, CuS-K and CuS-Q NPs were synthesized with some modifications according to a previous report.[38] Both of the NPs were well-dispersed and have an ultra-small size (**Figure 1**a,b) with an average diameter of 4.23 nm for CuS-K NPs and 2.93 nm for CuS-Q NPs (Figure S3, Supporting Information). This feature was in favor of ensuring deep tumor tissue penetration efficiency. Compared to the negative zeta potential (−2.62 mV) of control CuS NPs prepared in the absence of peptides, the zeta potentials of CuS-K NPs and CuS-Q NPs are significantly higher (22.83 and 19.87 mV respectively) (Figure 1c), indicating the successful synthesis of CuS-K NPs and CuS-Q NPs. The X-ray diffraction (XRD) patterns also revealed that the CuS-K NPs and CuS-Q NPs possessed characteristic peaks, as per the standard hexagonal crystal structure of CuS (JCPDS 060464) (Figure S4, Supporting Information). The transmission electron microscope (TEM) images of Lipo@CuS-K NPs and Lipo@CuS-Q NPs, captured without negative staining (Figure 1d,e) indicated the presence of CuS-K NPs and CuS-Q NPs as ultra-small dark dots within the liposomes, suggesting the successful loading of CuS-K NPs and CuS-Q NPs into the liposomes (Lipo@CuS-K or Lipo@CuS-Q). Additionally, the dynamic light scattering (DLS) analysis pointed out that Lipo@ICG@CuS-K NPs and Lipo@ICG@CuS-Q NPs possessed a hydrodynamic size of ≈140 nm, which is obviously larger than that of the original liposome (≈115 nm) (Figure 1f). Through loading into the liposome, the CuS-K and CuS-Q NPs could not be easily cleared from the blood circulation, facilitating the accumulation, and retention of more CuS NPs in the tumor site. The remarkable absorption bands in the UV–vis-NIR spectra between 800-1350 nm and 600–850 nm demonstrated the successful loading of CuS-K/Q and ICG into liposomes (Figure 1g), laying the foundation for the combination of PTT and PDT of the as-prepared NPs for anticancer application. Considering the crucial role of PTT in combined tumor therapy, the photothermal performance of Lipo@ICG@CuS-K NPs, and Lipo@ICG@CuS-Q NPs was measured. The photothermal effect of Lipo@ICG NPs was also tested due to the certain photothermal ability of ICG. The temperature of Lipo@ICG NPs increased by ≈12.4 °C, slightly higher than H_2O (4.9 °C). In strong comparison, the temperature of the Lipo@ICG@CuS-K NPs and Lipo@ICG@CuS-Q NPs systems increased to ≈45 °C, raising ≈22.2 and 23.8 °C,

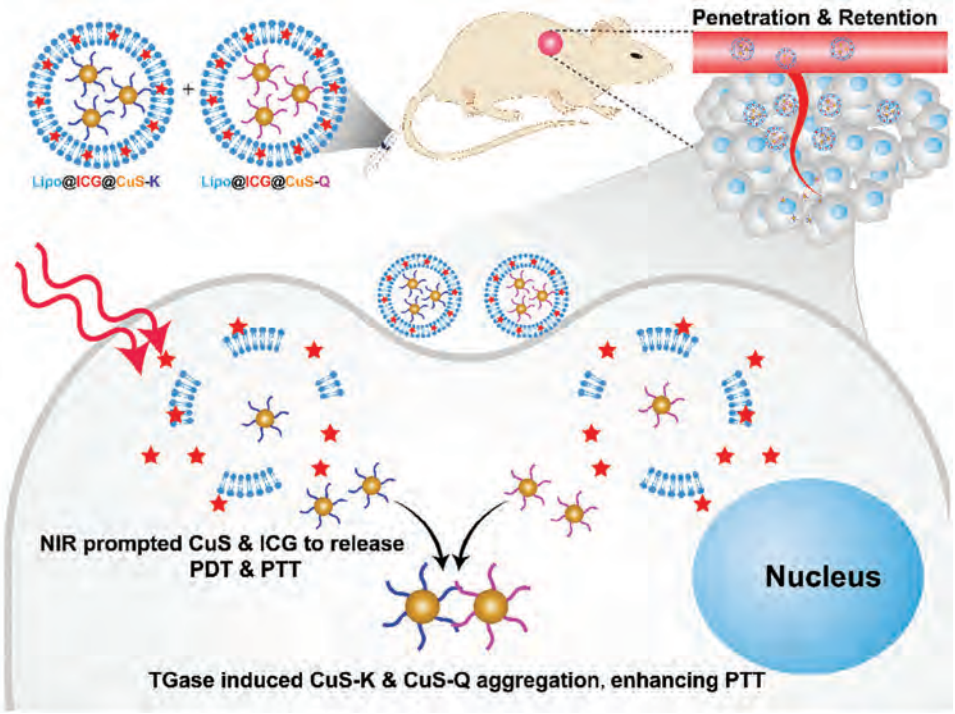

Scheme 1. NIR light and TGase triggered penetration and retention of nanoparticles for enhanced PTT &PDT.

respectively (Figure 1h), which could be attributed to the good photothermal conversion efficiency of CuS-K NPs (44.1%) and CuS-Q NPs (46.8%) (Figure S5, Supporting Information). In addition, CuS-K and CuS-Q showed good photothermal stability during five irradiation/cooling cycles (Figure S6, Supporting Information). The good heating capacity of CuS-K and CuS-Q NPs could induce the disintegration of the thermosensitive liposomes and promote the release of the cargoes, as evidenced by the obvious collapse of Lipo@CuS-K and Lipo@CuS-Q NPs in the TEM images and the concomitant release of CuS (Figure S7, Supporting Information). The above results suggested the successful synthesis of Lipo@ICG@CuS-K NPs and Lipo@ICG@CuS-Q NPs, the good photothermal performance, the thermosensitive collapse and the controllable cargo release.

2.2. Penetration and Aggregation In Vitro and In Vivo

The anticancer efficacy depends mainly on the dose of drugs delivered to the tumor site. However, the abnormal vasculature, extracellular matrix, and high interstitial fluid pressure greatly hinder the efficient penetration and subsequent accumulation of nanomedicines into the deep tumor. Therefore, the penetration and aggregation of anticancer drugs were crucial for efficient tumor therapy. Here, A375-derived multicellular spheroids were used to evaluate the penetration capacity of the synthesized NPs. The multicellular spheroids were incubated with the Lipo@CuS-K and Lipo@CuS-Q NPs labeled with fluorescein isothiocyanate (FITC), respectively. From the confocal laser scanning microscopy (CLSM) images (**Figure** 2a), the fluorescence was distributed throughout the spheroids, and the fluorescence intensity near the center was even stronger than that at the edge, indicating that Lipo@CuS-K NPs and Lipo@CuS-Q NPs have good penetration abilities. The average fluorescence intensity on the inset line further supported this result (Figure 2b). The penetration abilities of Lipo@CuS-K NPs and Lipo@CuS-Q NPs were then investigated in vivo. The distribution area of CuS NPs (green fluorescence) in the tumor tissue was considerably larger than that of liposomes (red fluorescence), whether Lipo@CuS-K NPs or Lipo@CuS-Q NPs (Figure 2c,e), which can be attributed to "the binding site barrier effect" of liposomes (labeled with DiI). The quantitative analysis results further revealed the good penetration of CuS-K NPs (≈two-fold than liposome) and CuS-Q NPs (≈1.5-fold than liposome) (Figure 2d,f). The above in vitro and in vivo results both demonstrated the good penetration abilities of CuS-K and CuS-Q NPs.

However, small CuS NPs can hardly accumulate at the tumor site, which inevitably limits the PTT efficacy. It is believed that the aggregated NPs should exhibit enhanced PTT activity.[39] Therefore, the responsive aggregation of CuS-K NPs with CuS-Q NPs was evaluated in vitro and in vivo. As shown in Figure S8 (Supporting Information), the CuS-K NPs and CuS-Q NPs clearly aggregated after co-incubation with TGase, which is very different from the monodispersed CuS-K NPs or CuS-Q NPs. The aggregates exhibited excellent photothermal capacity compared to the unaggregated mixture of CuS-K NPs and CuS-Q NPs (Figure S9, Supporting Information). In addition, the aggregation behavior was also observed at the cellular level by TEM. Dispersed CuS-K NPs or CuS-Q NPs could be clearly seen in A375 cells after incubation, but when the two types of NPs were co-incubated with cells together, there was a high degree of aggregation due to the overexpressed TGase in A375 cells (**Figure** 3a). The

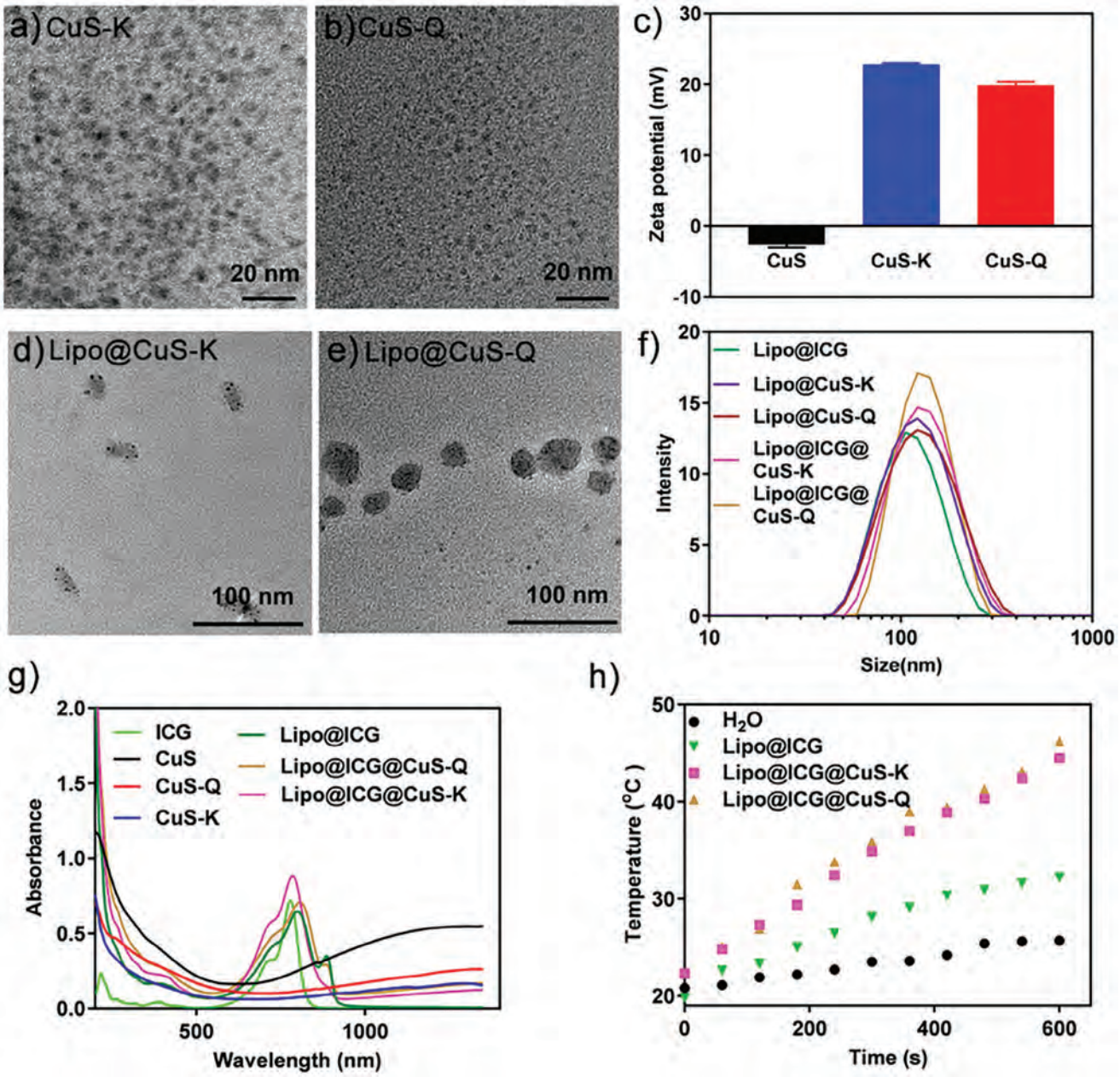

Figure 1. TEM images of a) CuS-K NPs, b) CuS-Q NPs, and c) Zeta potential of CuS NPs, CuS-K NPs, and CuS-Q NPs. TEM images of d) Lipo@CuS-K NPs, and e) Lipo@CuS-Q NPs. f) Hydrodynamic size of different samples. g) UV absorption spectra of different samples. h) Heating curves of H_2O, Lipo@ICG NPs, Lipo@ICG@CuS-K, and Lipo@ICG@CuS-Q NPs irradiated by the 808 nm NIR laser (0.8 W cm^{-2}).

aggregation and retention behavior was further investigated in vivo. From the colocalization analysis results of CuS-K and CuS-Q NPs, it suggested that FITC-labeled CuS-K NPs and rhodamine (RB)-labeled CuS-Q NPs were preferentially distributed and aggregated in the same area of tumor tissues (Figure 3b). The retention of CuS-K and CuS-Q NPs induced by TGase-triggered aggregation was also explored. The tumor tissues showed stronger fluorescence in the Lipo@CuS-K&Q group than in the Lipo@CuS-K or Lipo@CuS-Q groups alone (Figure 3c) after 24 h of injection, suggesting excellent retention for effective therapy. Quantitative analysis further confirmed the results (Figure 3d). The above results indicated that CuS-K and CuS-Q NPs possessed good penetration ability and could aggregate in response to the overexpressed TGase in tumor cells, thus significantly enhancing retention.

2.3. In Vitro Anticancer Effect

To evaluate the in vitro anticancer effect, we first investigated the cellular uptake of NPs. Lipo@CuS-K NPs and Lipo@CuS-Q NPs labeled with DiI were incubated with A375 cells for

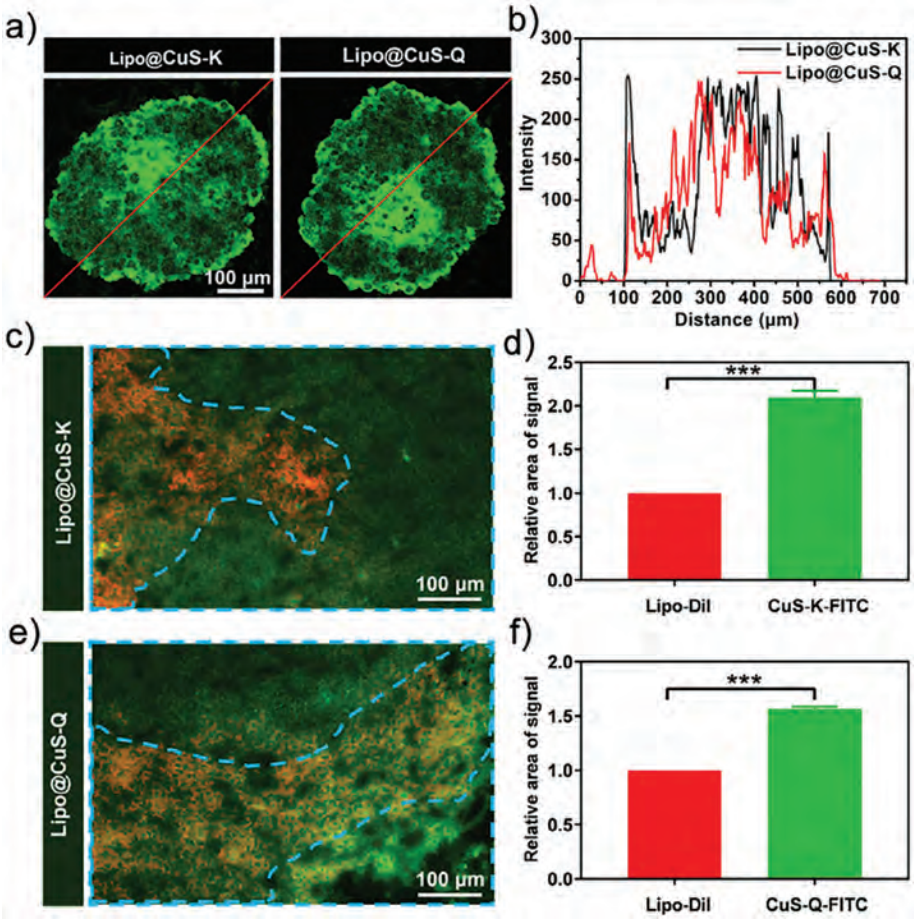

Figure 2. a) Penetration of FITC labeled Lipo@CuS-K NPs and Lipo@CuS-Q NPs in A375 multicellular spheroids after 4 h incubation. b) Fluorescence intensity of the line on the fluorescence images at 150 μm scanning depth. c) Distribution of CuS-K-FITC loaded Lipo-DiI and e) CuS-Q-FITC loaded Lipo-DiI in the A375 tumor tissues following intratumoral injection (n = 3). Image-based quantification analysis of distribution area of d) Lipo-DiI@CuS-K-FITC and f) Lipo-DiI@CuS-Q-FITC.

fluorescence imaging. As expected, the apparent red fluorescence in the cells indicated that these two types of NPs could be effectively taken up by A375 cells (**Figure** 4a). The quantitative flow cytometry study shows stronger DiI signals from the NPs treatment groups, further demonstrating the efficient uptake of NPs by A375 cells (Figure 4b). The cytotoxicity of the two types of NPs was evaluated, and the results showed that the cell viability remained above 80% when the concentration of NPs increased to 8 μg mL^{-1}, indicating the good cytocompatibility of the NPs (Figure 4c). In strong comparison, the cell viability decreased significantly (≈14%) upon 808 nm NIR laser irradiation of the two types of NPs and the viability even decreased to ≈8% for the treatment with the mixture of the two types of NPs, which can be attributed to the apparent in situ aggregation of the NPs in response to the intracellular TGase and the corresponding enhancement of the PTT effect (Figure 4d). Furthermore, the results of the intracellular ROS suggested that the ICG released from the nanosystem could also exert the enhanced PDT effect in the Lipo@ICG@CuS-K&Q group (Figure S10, Supporting Information). The therapeutic effect was further demonstrated by live/dead cell evaluation with calcein-AM/PI staining and apoptosis analysis with annexin V-FITC/PI double staining assays, respectively. The live/dead cell staining results showed that the Lipo@ICG@CuS-K&Q group exhibited a much stronger red fluorescence signal than other groups (Figure 4e), revealing its excellent therapeutic effect. The apoptosis evaluation results obtained by flow cytometric analysis showed that the apoptotic and necrotic A375 cells were 87% for the Lipo@ICG@CuS-K group and 87.5% for the Lipo@ICG@CuS-Q group, which were lower than the Lipo@ICG@CuS-K&Q group (90.2%) (Figure 4f). This tend was consistent with the results of the resazurin assay and live/dead cell staining. All these results showed that the Lipo@ICG@CuS-K&Q group had better cytotoxicity, which could be attributed to the aggregation of CuS-K NPs and CuS-Q NPs in response to TGase and then the enhanced PTT and PDT effects.

2.4. In Vivo Anticancer Efficacy

Inspired by the in vitro therapeutic results that the Lipo@ICG@CuS-K&Q NPs could effectively aggregate intracellularly and kill A375 cells efficiently under NIR laser irradiation, A375-bearing mice were selected to evaluate the in

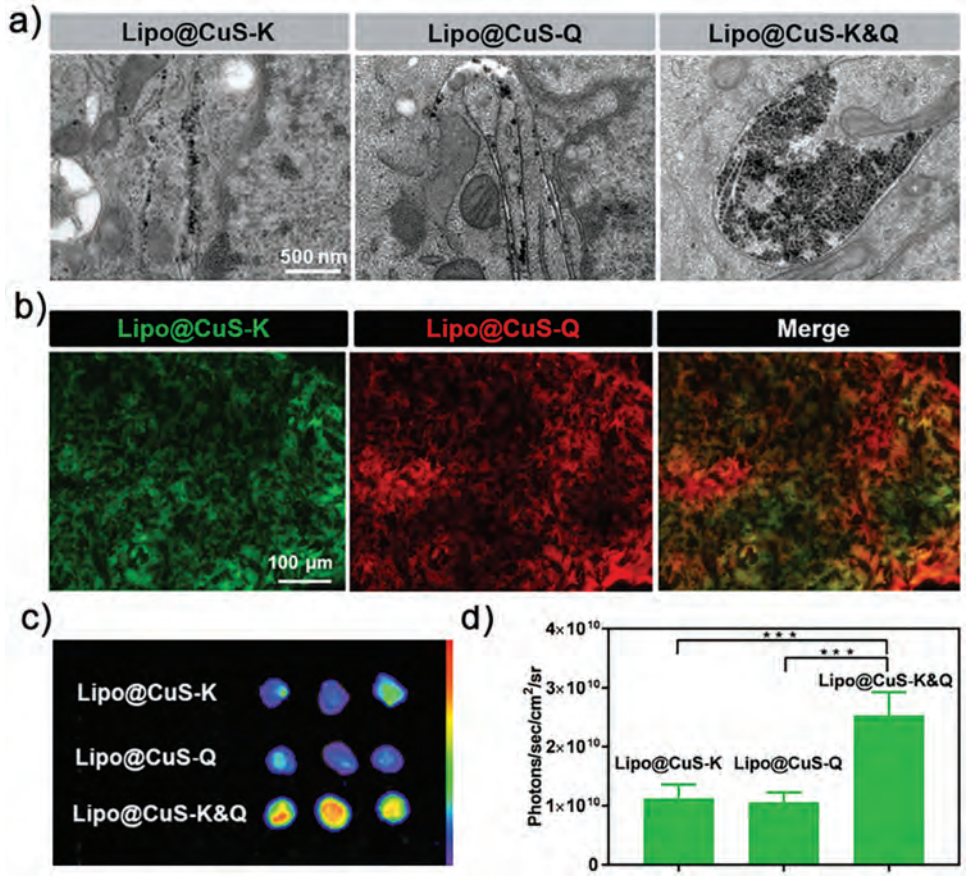

Figure 3. a) Representative TEM images of Lipo@CuS-K NPs, Lipo@CuS-Q NPs, and Lipo@CuS-K&Q NPs incubated in A375 cells. b) Co-localization of Lipo@CuS-K NPs and Lipo@CuS-Q NPs in tumor tissues (n = 3). c) Representative images and d) quantitative analysis of aggregation and retention at tumor tissues irradiated by the 808 nm NIR laser (1.0 W cm^{-2}) after intravenous injection 24 h (n = 3).

vivo performance of Lipo@ICG@CuS-K&Q NPs for enhanced PTT and PDT efficacy. First, in vivo imaging was performed to evaluate the accumulation of the as-prepared nanosystem at the tumor site after injection at different time points. As shown in **Figure** 5a, the fluorescence gradually increased with time, and the signal intensity at 24 h post-injection was ≈1.84-fold higher than that at 2 h (Figure 5b), suggesting the efficient accumulation of the nanosystem at the tumor site. Furthermore, *ex vivo* imaging of the tumor and major organs showed the strongest signal intensity in the tumor tissue, and quantitative analysis further confirmed the excellent tumor accumulation of the nanosystem (Figure 5c). Moreover, the results of photothermal imaging (Figure S11, Supporting Information) showed that the temperature of Lipo@ICG@CuS-K&Q group increased to ≈59 °C, ≈7 °C higher than that of the Lipo@ICG@CuS-K or Lipo@ICG@CuS-Q group, suggesting that the aggregation enhanced the photothermal performance. When the tumor size reached ≈100 mm^3 the mice were divided into the following four groups: (1) PBS (saline), (2) Lipo@ICG@CuS-K group, (3) Lipo@ICG@CuS-Q group, and (4) Lipo@ICG@CuS-K&Q group. NIR laser irradiation was performed after 24 h post-injection. To quantify the effectiveness of the treatment effects, tumor volume was recorded every other day. Compared with the control group, the Lipo@ICG@CuS-K and Lipo@ICG@CuS-Q groups showed efficient tumor inhibition with slow tumor growth. More importantly, the Lipo@ICG@CuS-K&Q group exhibited a much stronger anti-tumor effect than the Lipo@ICG@CuS-K group and the Lipo@ICG@CuS-Q group due to the aggregation of CuS-K NPs and CuS-Q NPs to enhance the PTT and PDT efficiency (Figure 5d). In addition, the side effects of the synthesized NPs were evaluated by monitoring the body weight of the experimental mice (Figure 5e). No obvious weight loss or abnormalities were observed, indicating that the NPs had no significant body toxicity. Moreover, micrographs of H&E-stained tumor sections showed the most severe tumor cell damage in the Lipo@ICG@CuS-K&Q group, while the other groups were either not significantly affected or only partially destroyed. Furthermore, the TUNEL staining results showed the better anti-tumor effect of the Lipo@ICG@CuS-K&Q group, with stronger fluorescence than other groups indicating more apoptotic cells (Figure 5f). In addition, the in vivo biosafety of these NPs was evaluated by collecting the major organs of the treated mice after 14 days, including heart, liver, spleen, lung, and kidney. H&E staining analysis showed no significant toxicity or side effects in the major organs (Figure S12, Supporting Information). Taken together, the evidence strongly supports the idea that aggregation of NPs in response to TGase plays a vital role in tumor therapy.

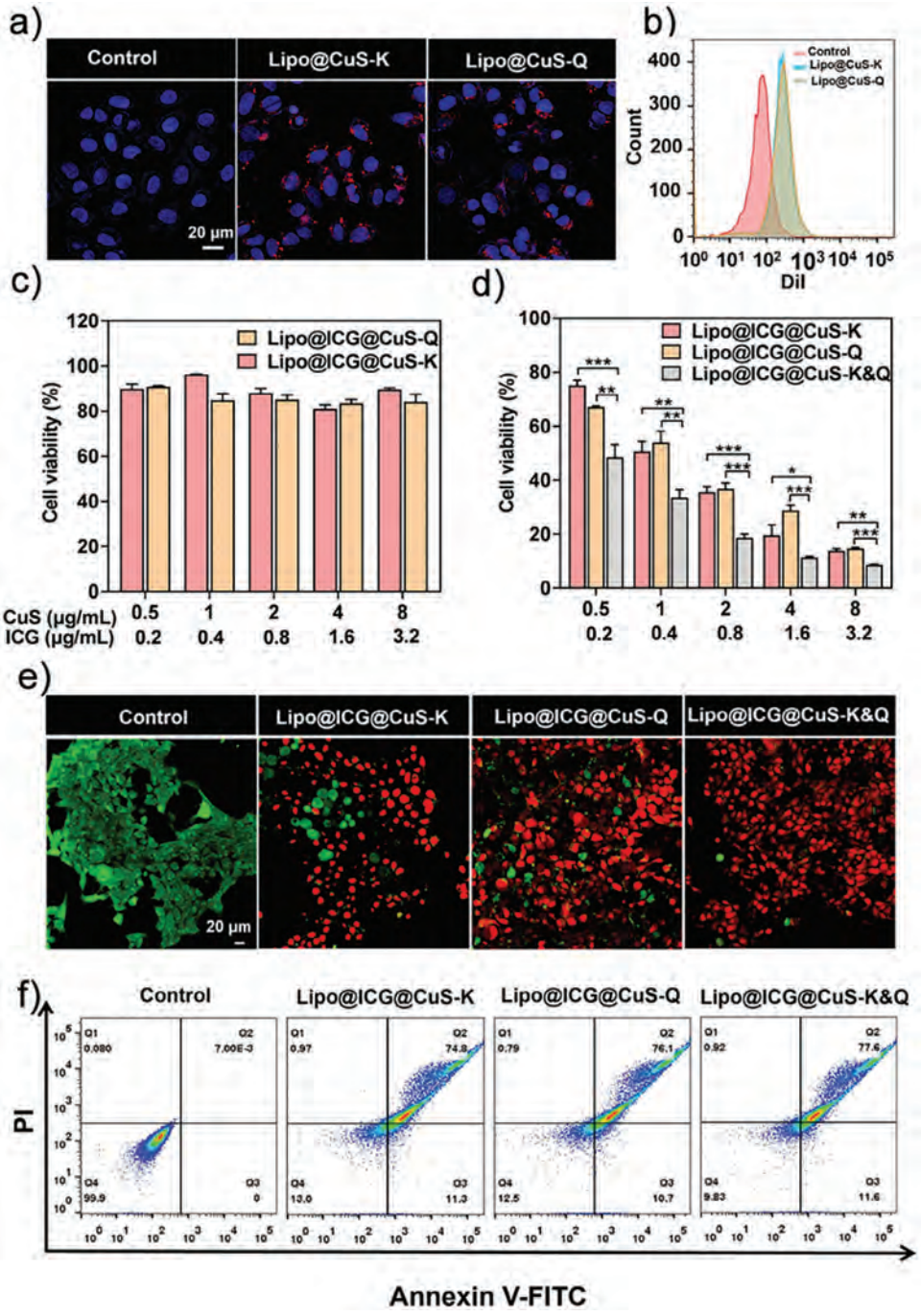

Figure 4. a) Cellular uptake and b) flow cytometry analysis of Lipo@CuS-K NPs and Lipo@CuS-Q NPs. c) Biocompatibility of CHO cells treated with different concentration of Lipo@ICG@CuS-K and Lipo@ICG@CuS-Q. d) Cell viability of A375 cells treated with different concentration of Lipo@ICG@CuS-K, Lipo@ICG@CuS-Q and Lipo@ICG@CuS-K&Q with 808 nm NIR laser irradiation at 0.8 W cm^{-2}. e) Live (green)/dead (red) staining, and f) apoptosis analyzed via flow cytometry of A375 cells with 808 nm NIR laser irradiation at 0.8 W cm^{-2}.

3. Conclusion

In summary, we have constructed a NIR light-triggered nanosystem to enhance NPs penetration and retention through the in situ aggregation of ultra-small CuS NPs in the tumor in response to intracellular TGase. CuS NPs were heated by the NIR laser, which caused the liposome to break apart and release CuS NPs and ICG that could efficiently penetrate deep tumors. Additionally, the released CuS NPs could respond to TGase in the tumor cells and aggregate in situ to further enhance PTT and PDT efficiency. The improved PTT and PDT effects of the nanosystem produced excellent tumor therapeutic efficacy, and in vitro and in vivo

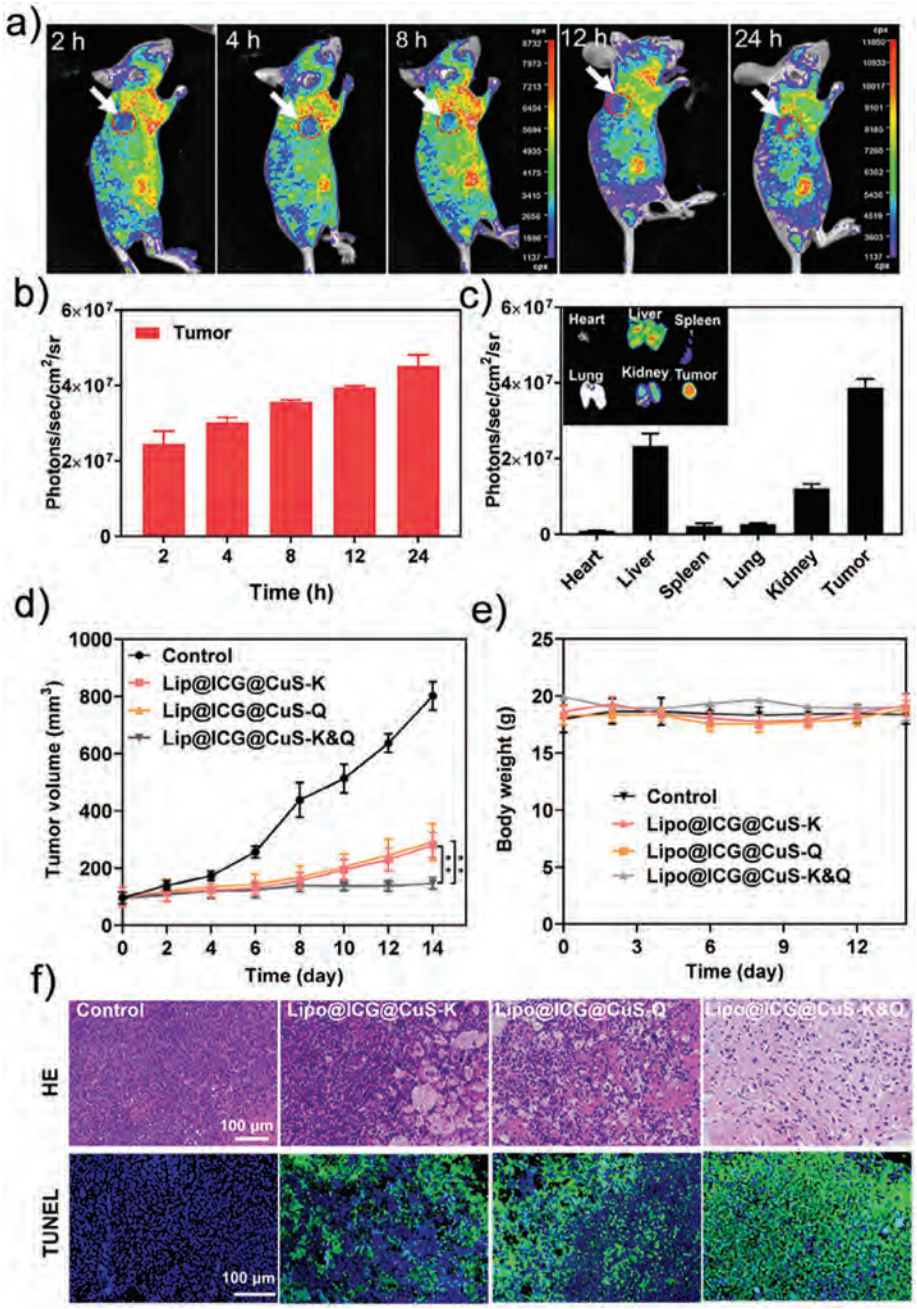

Figure 5. a) Fluorescence imaging of A375 tumor (white arrow) with time after intravenous injection of Lipo@ICG@CuS-K&Q labeled by DiI. b) Quantitative analysis of mean fluorescence intensity in tumor at various points in time. c) Fluorescence imaging and quantification analysis of biodistribution of Lipo@ICG@CuS-K&Q in different tissues. d) Tumor volume changes, e) Body weight changes and f) H&E and TUNEL staining of different groups after different treatments (n = 5).

experiments supported these findings. It is envisioned that this smart nanosystem would be an attractive and versatile platform to explore more possibilities in nanotherapeutics. Moreover, we believe that this work will inspire researchers to create new nanosystems with prolonged blood circulation time, better penetration, and retention, as well as multimodal synergetic therapy, in order to realize satisfactory therapeutic efficacy in the treatment of tumors.

4. Experimental Secction

Chemicals and Reagents: Dipalmitoylphosphatidylcholine (DPPC) and 1,2-distearoyl-sn-glycero-3-phosphoethanolamine-N-[methoxy(polyethylene glycol)−2000] (DSPE-PEG2000) were purchased from Shanghai Ponsure Biotech, Inc. Cholesterol was purchased from Shanghai Yuanye Bio-Technology Co. Ltd. Indocyanine green was purchased from J&K Scientific. Copric chloride dehydrate ($CuCl_2{\cdot}2H_2O$) and TGase were purchased from Aladdin Ltd. (Shanghai, China). Fluorescein

isothiocyanate (FITC) was purchased from Solarbio. 2-Chlorotrityl chloride resin, Fmoc-Cys(Trt)-OH, Fmoc-Arg(Pbf)-OH, Fmoc-Lys(Boc)-OH, Fmoc-Gln(Trt)-OH, and O-(benzotriazol-1-yl)-N,N,N′,N′-tetramethyluronium hexafluorophosphate (HBTU) were purchased from GL Biochem (Shanghai, China).

Cell Lines and Animals: Human malignant melanoma cell line A375 and CHO Chinese hamster ovary cell line were obtained from the cell bank of the Chinese Academy of Sciences. A375 cells and CHO cells were cultured in DMEM high glucose medium (Gibco), containing 10% fetal bovine serum (FBS) at 37 °C in a 5% CO_2 humidified environment incubator (Thermo Scientific, USA).

BALB/c female nude mice (6–8 weeks) were fed at 25 °C and 55% relative humidity. The A375 xenograft tumor model was produced by subcutaneous injection of 1×10^7 cells in 100 µL of DMEM high glucose medium into the backs of the mice. After the tumor volume grew to a size of roughly 100 mm^3 The treatment was initiated All animal procedures for this study were approved by the Institutional Animal Care Department of Henan Normal University.

Preparation of CuS NPs Modified by Peptides: PepK (CRKKKR) and PepQ (CRRQQR) were synthesized by solid phase peptide synthesis (SPPS) using 2-chlorotrityl chloride resin and the corresponding N-Fmoc protected amino acids with the side chains properly protected. 20% piperidine in DMF was used to deprotect the Fmoc group. Peptide chain growth was achieved according to the established Fmoc SPPS protocol. After the final coupling step, excess reagents were removed by a single wash with DMF for 5 min (5 mL per gram of resin), followed by five washes with dichloromethane (DCM) for 5 min (5 mL per gram of resin). The peptide derivative was cleaved using trifluoroacetic acid (TFA)/thioanisole/phenol/1,2-ethanedithiol/H_2O (87.5/5/2.5/2.5/2.5, v/v/v/v/v) for 3 h. After concentration of the solution using a rotary evaporator, the product obtained was washed with ice-cold diethyl ether.The crude product was then purified by HPLC and dried in a lyophilizer. The synthesis of CuS NPs was carried out as previously reported with slight modifications. Briefly, 0.1 mmol of $CuCl_2{\cdot}2H_2O$ was dissolved in 100 mL of distilled water, and 0.01 mmol of peptide K (CRKKKR) or Q (CRQQRR) was added and stirred for 30 min to obtain a homogeneous solution. Aqueous solution of thioacetamide (0.1 mmol) was added dropwise, and the whole solution was heated at 50 °C for 2 h to promote nanoparticle growth. The solution was further purified by centrifugation. For FITC labeling of CuS NPs, 1 mL of FITC-PEG2000-SH (10 mg L^{-1}, MW = 2000) was sonicated with the CuS NPs (5 mg L^{-1}) for 30 min. The mixture was then stirred overnight, and the CuS NPs were collected after three washes to remove excess FITC-PEG2000-SH.

Preparation of ICG-Loaded Liposomes: To obtain an ICG-loaded liposome, the mixture of DPPC, cholesterol, DSPE-PEG2000, and ICG in a molar ratio of 18:6:1.5:1 was dissolved in chloroform and then dried under a rotary evaporator. The dried lipid film was then hydrated with PBS, followed by extrusion through 400 , 200 , and 100 nm polycarbonate filters 20 times, each. The resulting Lipo@ICG was concentrated using an ultrafiltration device with a molecular weight cut-off of 30 kDa (Millipore) for further use.

Loading of CuS NPs into Liposomes: The resulting lipid film of Lipo@ICG was fully hydrated with 2 mL of aqueous dispersion of CuS NPs (2 mg mL^{-1}) for 1 h at 60 °C. The mixture was then sonicated for 30 min to ensure successful loading of CuS NPs into Lipo@ICG. After removing the free CuS NPs by centrifugation, the pellet was resuspended in PBS. The resulting solution was extruded sequentially through 400 , 200 , and 100 nm polycarbonate filters for further use. The encapsulation content of CuS NPs was determined by ICP-MS analysis.

Characterization: TheTEM samples were prepared by dropping 10 µL of solution on the copper grids, and the images were obtained using a JEM-100CX-II transmission electron microscope. DLS and zeta potential were measured using the Zetasizer Nano ZS90. UV-vis-NIR spectra were measured with a Lambda 950. High resolution mass spectra were obtained using an autoflex speed MALDLTOF/TOF.

Measurement of Photothermal Performance: To analyze the photothermal performance of CuS NPs, Lipo@ICG NPs, Lipo@ICG@CuS-K NPs, and Lipo@ICG@CuS-Q NPs, the aqueous suspensions (50 µg mL^{-1} CuS, 20 µg mL^{-1} ICG) of the above samples were exposed to an 808 nm NIR laser (0.8 W cm^{-2} 10 min). During the experimental process, the temperature was recorded every 60 sec using a high-precision thermocouple sensor. To calculate the photothermal conversion efficiency, the suspension was allowed to cool naturally after removal of the laser. The photothermal conversion efficiency was determined using the method reported by Roper and coworkers.[40]

Analysis of Cellular Uptake and Sample Distribution: A375 cells were seeded at 5×10^4 in glass-bottom dishes and cultured for 48 h. Fresh medium (without FBS) containing Lipo@CuS-K or Lipo@CuS-Q (16.9 µg mL^{-1} for CuS NPs) labeled with DiI was added and cultured for 6 h. The cells were washed three times with PBS and fixed with 4% paraformaldehyde solution for 20 min, followed by staining with DAPI for 15 min. The distribution of NPs in the cells was observed by confocal microscopy.

Evaluation of Penetration by A375 Cell Spheroids: A375-based multicellular spheroids were prepared as reported elsewhere with some modifications.[41] Briefly, 50 µL of DMEM medium containing 1% (w/v) agarose was added and solidified in each well of 96-well microplates. Then, 1×10^4 A375 cells per well were seeded and cultured for 4,5 days to obtain 3D multicellular tumor spheroids. The spheroids were carefully transferred to glass bottom dishes, where CuS-K/Q-FITC-loaded liposomes were added and incubated for 4 h. Finally, the cell spheroids were observed under a laser confocal microscope (OLYMPUS FV1200).

Evaluation of Intratumoral Penetration: Tumor-bearing mice were administered 20 µL of CuS-K/Q-FITC-loaded Lipo-DiI (CuS equivalent 5 mg Kg^{-1}) by intratumoral injection using an automated syringe. Mice were sacrificed 2 h after administration, and tumors were harvested and frozen in OCT. Whole tumor tissues were then cryosectioned at 10 µm thickness (Leica Biosystems), and a series of sections were imaged using confocal microscopy. The background signal of the tissues was compensated by the use of an untreated tumor tissue. The maximum coverage area of the fluorescent signal in the tumor tissues was chosen as a representative image to determine the penetration distance. Image-based quantification analysis was performed using Image J software.

TEM Observation of the NP's In Situ Aggregation in A375 Cells: The A375 cells cultured in a culture dish were treated with Lipo@CuS-K, Lipo@CuS-Q, or Lipo@CuS-K&Q for 6 h after adhesion to the dish. Cells were collected and washed with PBS. The cells were then fixed with glutaraldehyde for 1 h at room temperature to obtain the samples. The samples were processed and imaged.

Colocalization Evaluation: The CuS-K NPs were labeled with HS-PEG2000-FITC, and the CuS-Q NPs were labeled with HS-PEG2000-RB (Rhodamine b). The tumor-bearing mice were then administered 20 µL Lipo-DiI@CuS-K-FITC and Lipo-DiI@CuS-Q-RB (CuS NPs equivalent to 5 mg Kg^{-1}) by intratumoral injection using an automated syringe. Tumor tissue sections were prepared as described in 4.10 and imaged by confocal microscopy.

Accumulation and Retention of NPs in Tumor Tissue: The CuS-K and CuS-Q NPs were labeled with HS-PEG2000-FITC. The tumor-bearing mice were then administered Lipo@ICG@CuS-K-FITC, Lipo@ICG@CuS-Q-FITC, and Lipo@ICG@CuS-K&Q-FITC (CuS NPs equivalent to 5 mg Kg^{-1}) by intravenous injection, respectively. The tumor site was then irradiated with 808 nm NIR laser irradiation (1.0 W cm^{-2} 10 min) at 24 h post-treatment, and the tumor tissues were imaged using IndiGo software.

Detection of Intracellular ROS: Dichlorofluorescein diacetate (DCFH-DA) was used to detect intracellular ROS levels. Cells were incubated with NPs for 6 h. After washing with PBS, the DCFH-DA (10 rhodamine (RB)µM) was added and incubated for 20 min. The cells were again washed three times with PBS. Prior to confocal microscopy, the cells were exposed to NIR laser irradiation (808 nm, 0.8 W cm^{-2}) for 2 min.

Evaluation of Cytocompatibility and Cytotoxicity: Cytocompatibility and cytotoxicity were assessed using the standard resazurin method. Briefly, CHO cells or A375 cells (5×10^3 cells/well) were seeded into 96-well plates. After plate attachment, CHO cells were incubated with Lipo@ICG@CuS-K or Lipo@ICG@CuS-Q at CuS NPs concentrations of 0.5, 1, 2, 4, and 8 µg mL^{-1} for 24 h, and cytocompatibility was assessed using a standard resazurin method (Ex = 540 nm, Em = 590 nm). For

cytotoxicity evaluation, A375 cells were incubated with Lipo@ICG@CuS-K or Lipo@ICG@CuS-Q at the equivalent CuS NPs concentrations of 0.25, 0.5, 1, 2, and 4 μg mL^{-1}, respectively. Each well of the 96-well plates was then exposed to 808 nm NIR laser irradiation (808 nm, 0.8 W cm^{-2}) for 5 min. After a further 12 h incubation, cytotoxicity was assessed using the standard resazurin method. A LIVE/DEAD assay was also performed to assess the therapeutic efficacy of the samples. After treatment with Lipo@ICG@CuS-K, Lipo@ICG@CuS-Q, or Lipo@ICG@CuS-K&Q for 24 h, the cells were incubated with Calcein-AM (4 μM)/PI (4.5 μM) for 20 min, washed with PBS, and imaged by laser confocal microscope. For the cell apoptosis assay, A375 cells were harvested and washed with PBS after treatment with Lipo@ICG@CuS-K, Lipo@ICG@CuS-Q, or Lipo@ICG@CuS-K&Q for 6 h. The cells were then resuspended in 100 μL of Annexin V binding buffer, co-incubated with Annexin V-FITC (5 μL) and PI (5 μL) for 15 min, and analyzed by flow cytometer (BD LSR-Fortessa, USA).

In Vivo and Ex Vivo Imaging: To investigate the accumulation of the nanosystem at the tumor site in vivo, A375 tumor-bearing mice were injected intravenously with Lipo@ICG@CuS-K&Q labeled with DiI. The mice were imaged at regular intervals. Mice were also sacrificed 24 h after injection, and major organs and tumors were harvested and imaged.

In Vivo Photothermal and Photodynamic Therapy and Tissue Evaluation: In this trial, female BALB/c nude mice bearing A375 subcutaneous tumors were randomly divided into four groups: PBS, Lipo@ICG@CuS-K NPs (5 mg Kg^{-1} CuS, 0.92 mg Kg^{-1} ICG), Lipo@ICG@CuS-Q NPs (5 mg Kg^{-1} CuS, 0.92 mg Kg^{-1} ICG), and Lipo@ICG@CuS-K&Q NPs (5 mg Kg^{-1} CuS, 0.92 mg Kg^{-1} ICG). NPs were administered systemically to the mice when tumor volumes reached ≈100 mm^3 After 24 h of injection, an 808 nm NIR laser was used to irradiate the tumors for 10 min (1.0 W cm^{-2}). Tumor volumes and body weights were recorded every two days until the end of treatment. Hematoxylin and eosin (H&E) staining analysis was performed after 14 days of treatment. H&E staining of tumor tissue was performed according to standard procedures. First, the tumors were isolated, fixed in 4% paraformaldehyde, and then embedded in paraffin. The paraffin-embedded tumor tissues were cut into 5 μm thick slices. The sections were then stained with H&E for histopathological examination. TUNEL staining of the tumor sections was also performed according to the manufacturer's instructions for the TUNEL Apoptosis Assay Kit (Beyotime Biotechnology). In addition, the histocompatibility of the samples was examined by H&E staining with major organs (heart, liver, spleen, lung, and kidney).

Statistical Analysis: Student's unpaired t-test was used for statistical analysis between two groups of independent data. Where multiple comparisons were involved, one-way or two-way analysis of variance was used as appropriate. Differences were considered statistically significant at $p < 0.05$. Results were presented as mean ± SEM.

Supporting Information

Supporting Information is available from the Wiley Online Library or from the author.

Acknowledgements

F.G. and L.Z. contributed equally to this work. This work was financially supported by the National Natural Science Foundation of China (21771058 and 21877027) and the Natural Science Foundation of Henan (212300410009 and 232300421302), the 111 Project (No. D17007), the Program for Science & Technology Innovation Talents in Universities of Henan Province (No. 23HASTIT002) and the Foundation of Henan Educational Committee (23A150021).

Conflict of Interest

The authors declare no conflict of interest.

Data Availability Statement

The data that support the findings of this study are available in the supplementary material of this article.

Keywords

aggregate, combined anti-tumor effect, nanomedicines, penetrate, retention

Received: October 4, 2023
Published online: November 21, 2023

[1] Z. Li, X. Shan, Z. Chen, N. Gao, W. Zeng, X. Zeng, L. Mei, *Adv. Sci.* **2020**, *8*, 2002589.
[2] H. Cabral, Y. Matsumoto, K. Mizuno, Q. Chen, M. Murakami, M. Kimura, Y. Terada, M. R. Kano, K. Miyazono, M. Uesaka, N. Nishiyama, K. Kataoka, *Nat. Nanotechnol.* **2011**, *6*, 815.
[3] S. Kunjachan, R. Pola, F. Gremse, B. Theek, J. Ehling, D. Moeckel, B. Hermanns-Sachweh, M. Pechar, K. Ulbrich, W. E. Hennink, G. Storm, W. Lederle, F. Kiessling, T. Lammers, *Nano Lett.* **2014**, *14*, 972.
[4] F. Xu, X. Huang, Y. Wang, S. Zhou, *Adv. Mater.* **2020**, *32*, 1906745.
[5] L. Gu, Z. Duan, X. Chen, X. Li, Q. Luo, A. Bhamra, D. Pan, H. Zhu, X. Tian, R. Chen, Z. Gu, H. Zhang, Z. Qian, Q. Gong, K. Luo, *Adv. Mater.* **2022**, *34*, 2200048.
[6] S. Ruan, C. Hu, X. Tang, X. Cun, W. Xiao, K. Shi, Q. He, H. Gao, *ACS Nano* **2016**, *10*, 10086.
[7] K. Yang, Y. Liu, Y. Wang, Q. Ren, H. Guo, J. B. Matson, X. Chen, Z. Nie, *Biomaterials* **2019**, *223*, 119460.
[8] Y. Zhang, F. Huang, C. Ren, J. Liu, L. Yang, S. Chen, J. Chang, C. Yang, W. Wang, C. Zhang, Q. Liu, X.-J. Liang, J. Liu, *Adv. Sci.* **2019**, *6*, 1801806.
[9] H. Xia, Y. Gao, L. Yin, X. Cheng, A. Wang, M. Zhao, J. Ding, H. Shi, *ChemBioChem* **2019**, *20*, 667.
[10] Z. Zhang, C. Ding, T. Sun, L. Wang, C. Chen, *Adv. Healthcare Mater.* **2023**, *12*, e2300153.
[11] A. Facchiano, F. Facchiano, *Amino Acids* **2009**, *36*, 599.
[12] T. Takeuchi, H. Tatsukawa, Y. Shinoda, K. Kuwata, M. Nishiga, H. Takahashi, N. Hase, K. Hitomi, *Am. J. Respir. Cell Mol. Biol.* **2021**, *65*, 319.
[13] S. Y. Cho, E. M. Jeong, J. H. Lee, H. J. Kim, J. Lim, C. W. Kim, D. M. Shin, J. H. Jeon, K. Choi, I. G. Kim, *Mol. Cells* **2012**, *33*, 235.
[14] R. L. Eckert, M. T. Kaartinen, M. Nurminskaya, A. M. Belkin, G. Colak, G. V. W. Johnson, K. Mehta, *Physiol. Rev.* **2014**, *94*, 383.
[15] H. Lortat-Jacob, I. Burhan, A. Scarpellini, A. Thomas, A. Imberty, R. R. Vivès, T. Johnson, A. Gutierrez, E. A. M. Verderio, *J. Biol. Chem.* **2012**, *287*, 18005.
[16] B. Spolaore, S. Raboni, A. A. Satwekar, A. Grigoletto, A. Mero, I. M. Montagner, A. Rosato, G. Pasut, A. Fontana, *Bioconjugate Chem.* **2016**, *27*, 2695.
[17] Z. Yuan, X. Gao, Y. Liu, Y. Li, X. Niu, J. Cao, X. Li, Y. Zhang, D. Tan, W. Wang, *Mater. Chem. Front.* **2019**, *3*, 1365.
[18] L.-L. Li, S.-L. Qiao, W.-J. Liu, Y. Ma, D. Wan, J. Pan, H. Wang, *Nat. Commun.* **2017**, *8*, 1276.
[19] S. Liu, X. Pan, H. Liu, *Angew. Chem., Int. Ed.* **2020**, *59*, 5890.
[20] Y. Liu, P. Bhattarai, Z. Dai, X. Chen, *Chem. Soc. Rev.* **2019**, *48*, 2053.
[21] M. Kim, J.-H. Lee, J.-M. Nam, *Adv. Sci.* **2019**, *6*, 1900471.
[22] D. Zhi, T. Yang, J. O'Hagan, S. Zhang, R. F. Donnelly, *J. Controlled Release* **2020**, *325*, 52.
[23] C. Murugan, V. Sharma, R. K. Murugan, G. Malaimegu, A. Sundaramurthy, *J. Controlled Release* **2019**, *299*, 1.

[24] H. Sun, Q. Zhang, J. Li, S. Peng, X. Wang, R. Cai, *Nano Today* **2021**, *37*, 101073.
[25] Z. Zheng, P. Yu, H. Cao, M. Cheng, T. Zhou, L. E. Lee, J. Ulstrup, J. Zhang, C. Engelbrekt, L. Ma, *Small* **2021**, *17*, e2103461.
[26] J. Li, Q. Cheng, L. Yue, C. Gao, J. Wei, Y. Ding, Y. Wang, Y. Zheng, R. Wang, *Nanoscale Horiz.* **2021**, *6*, 907.
[27] R. Cai, H. Xiang, D. Yang, K.-T. Lin, Y. Wu, R. Zhou, Z. Gu, L. Yan, Y. Zhao, W. Tan, *J. Am. Chem. Soc.* **2021**, *143*, 16113.
[28] Y. Huang, Y. Lai, S. Shi, S. Hao, J. Wei, X. Chen, *Chem Asian J.* **2015**, *10*, 370.
[29] K. Poudel, M. Gautam, S. G. Jin, H.-G. Choi, C. S. Yong, J. O. Kim, *Int. J. Pharm.* **2019**, *562*, 135.
[30] Q. Wu, G. Chen, K. Gong, J. Wang, F. Wang, *Matter* **2019**, *1*, 496.
[31] R. X. Zhang, H. L. Wong, H. Y. Xue, J. Y. Eoh, X. Y. Wu, *J. Controlled Release* **2016**, *240*, 489.
[32] J. M. Dabrowski, L. G. Arnaut, *Photochem. Photobiol. Sci.* **2015**, *14*, 1765.
[33] J. Xie, R. Liang, Q. Li, K. Wang, M. Hussain, L. Dong, C. Shen, H. Li, G. Shen, J. Zhu, J. Tao, *Acta Biomater.* **2022**, *142*, 264.
[34] G. Wan, B. Chen, L. Li, D. Wang, S. Shi, T. Zhang, Y. Wang, L. Zhang, Y. Wang, *Biomaterials* **2018**, *161*, 25.
[35] F. Gao, L. Jiang, J. Zhang, Y. Chang, W. Gao, L. Ding, G. Ma, X. Ma, Y. Guo, *ACS Mater. Lett.* **2023**, *5*, 1.
[36] T. Liu, R. Jin, P. Yuan, Y. Bai, X. Chen, *ACS Appl. Mater. Interfaces* **2019**, *11*, 28621.
[37] Y. Wu, Y. Gao, J. Su, Z. Chen, S. Liu, *Chem. Commun.* **2020**, *56*, 9008.
[38] Y. Li, W. Lu, Q. Huang, C. Li, W. Chen, *Nanomedicine* **2010**, *5*, 1161.
[39] J. Sheng, B. Ma, Q. Yang, C. Zhang, Z. Jiang, E. Borrathybay, *Int. J. Nanomed.* **2018**, *13*, 4291.
[40] D. K. Roper, W. Ahn, M. Hoepfner, *J. Phys. Chem. C* **2007**, *111*, 3636.
[41] J. Friedrich, C. Seidel, R. Ebner, L. A. Kunz-Schughart, *Nat. Protoc.* **2009**, *4*, 309.